https://doi.org/10.2352/EI.2025.37.9.IQSP-240

Building End-to-End deblur image quality evaluation simulation for Hybrid-EVS-CIS sensor images

Daisuke Saito, Kamal Rana, Zhiyao Yang, Wei Zhang, Bo Mu, Eiichi Funatsu;
OMNIVISION, Santa Clara CA/USA

Abstract

Event-based Vision Sensor (EVS) generates pixel-level and low-latency event data that is useful for reconstructing temporal components of images for deblurring. In this new application development, we need to know how EVS hardware parameters affect the natural motion scene image quality (IQ) to determine hardware specifications before starting design. To realize this approach, it is beneficial to build an End-to-End IQ simulation that runs from hardware simulations to natural motion scene IQ evaluation. Previously, we developed a Hybrid-EVS-CIS simulator to generate synthesized color rotation disk images and their event data fed into an image deblur block. Then image blurriness was evaluated by using the Blurred Edge Width metric (BEW). This paper proposes the extended IQ evaluation, which is an End-to-End IQ simulation for natural motion scenes. A simultaneous evaluation of blurriness and noise on images was verified by using Visual Information Fidelity and Detail Loss Metric. We also build a method to assess pixel-speed using BEW. Those IQ evaluation methods were the last pieces to realize End-to-End IQ simulation.

Introduction

Event-based Vision Sensor (EVS) detects the pixels that show a relative luminance change. This EVS function reduces the number of pixels to be read per frame, resulting in a faster readout than a CMOS image sensor (CIS) [1, 2]. This event data is useful for algorithms reconstructing high temporal components of images to complement CIS images, such as image deblurring, and video frame interpolation. These algorithms require appropriate event data for better quality of the generated image. Thus, we proposed an End-to-End image quality (IQ) simulation scheme to enable fast reliable IQ evaluation, in which circuit designers specify EVS hardware parameters by simulating the influence on the finished IQ prior to starting the hardware design. Our prior work developed a Hybrid-EVS-CIS simulator (Hybrid-simulator) generated Rolling-shutter (RS) CIS images and their event data to develop algorithms. The event data generation flow is shown in Fig. 1. The scene data was captured from a high-speed global-shutter camera (HS-GS images). HS-GS images were converted into photocurrents, which were employed in the EVS pixel circuit model to generate events. These generated events were collected by simulating the read-out circuit. The events were then fed into the deblur block, which utilized the Event-Double-Integral algorithm [3], along with the generated RS CIS images. We proposed the Blurred Edge Width (BEW) method using color-rotation-disk [4] to evaluate the blurriness of those deblurred images. However, because BEW was designed to test simple image features, it could not be directly applied to assess the quality of natural motion scenes, which was a missing component of End-to-End IQ simulation.

In this paper, we realized the natural motion scene IQ simulation as a building block of End-to-End IQ simulation shown in Fig. 2. The red boxes are the key items to perform IQ simulation, which are IQ metrics and ground truth images. To verify IQ metrics, first, we performed a deblurred images evaluation by using Visual Information Fidelity (VIF) [5] and Detail Loss Metric (DLM) [6] with RS ground truth images (RS-GT images). Second, we used BEW to assess pixel speed, which affects blurriness. The distribution of scene pixel speeds was compared between color rotation disk and natural motion scenes. Then we evaluated the correlation between BEW and VIF/DLM on color rotation disk images.

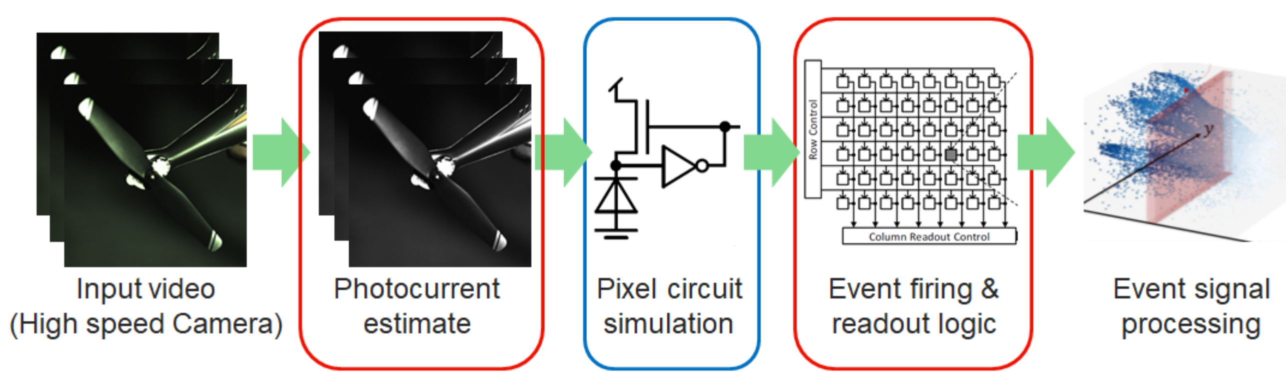

Figure 1: An illustrated pipeline of a Hybrid-EVS-CIS camera simulator reported in our prior work [7]. Event data and CIS images were generated from estimated photocurrent.

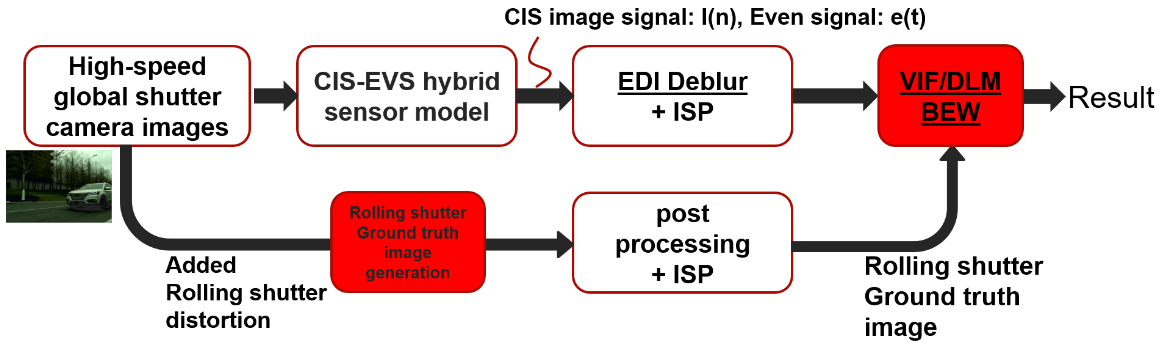

Figure 2: End-to-End IQ simulation. Red boxes are key items to build this pipeline.

VIF/DLM verification for deblurred images

Evaluation method

VIF and DLM are used in Video Multi-method Assessment Fusion (VMAF) [8] which is primarily aimed at evaluating video quality, particularly for videos encoded with various codecs. VIF is an image quality assessment index based on natural scene statistics and the concept of image information as perceived by the human visual system. DLM is the method employed to assess the loss of valuable visual information that impacts content visibility extracted from distorted images. Both VIF and DLM are full reference metrics that evaluate images against ground truth images. This time, we utilized VIF and DLM to assess blurriness and noise in deblurred images. These images were RS CIS images generated from HS-GS images in our End-to-End IQ simulation. No-blur RS-GT images were created using the same HS-GS images that were employed to synthesize deblurred images. The pixel values of the No-blur RS-GT images were made from several frames of HS-GS images according to RS read-out timing. The scenes used for this study are shown in Fig. 3.

Figure 3: Data set used for this study. Images were used for VIF/DLM validation by sweeping some circuit parameters.

We evaluated the effect of the EVS pixel circuit on deblurred images. During the generation of event data for image deblurring, we varied several circuit parameters that are part of the Hybrid-simulator's hardware parameters. The simulation conditions for CIS images used for deblurring were consistent across all experiments. We assessed blurriness and noise in the deblurred images using a combined score from VIF and DLM as a function of circuit parameters. This score was calculated by fusing VIF and DLM into a final metric through a Support Vector Machine regressor, which assigns weights to both VIF and DLM [9]. The final metric retained the strengths of both VIF and DLM and computed an overall score. The default settings in the VMAF development kit were employed to compute the VIF-DLM combined score for this experiment.

Moving scene evaluation

Figure 4 presents the evaluation results of the combined VIF-DLM scores for a synthesized deblurred moving car scene under low light conditions (20 lux). The event data for the image deblurring was generated by varying two circuit parameters. The first parameter, referred to as "Parameter a," relates to the latency of EVS pixel responses and the output noise. The second parameter, "Parameter b," is also associated with output noise. The effect of "Parameter b" was studied under two different conditions. One was the reference condition (black dots, Ref) and the other was a condition where "Parameter b" was ten times larger than the reference value (blue dots, Ref x 10).

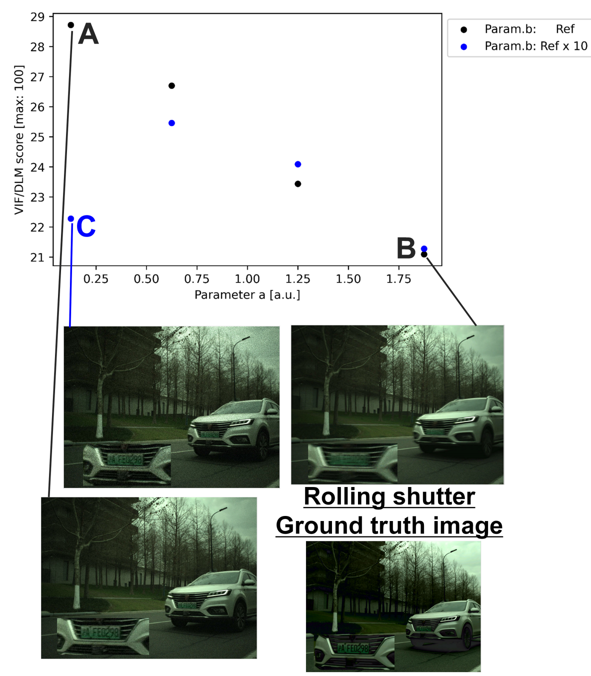

Figure 4: A detailed car moving scene analysis. These images were synthesized from a Hybrid-EVS-CIS simulator with two types of circuit parameters (Parameter a. and b.) at 20 Lux on the scenes. A blurriness in images degrades the VIF-DLM combined score. Noisy or blurred images show a lower VIF-DLM combined score.

The deblurred images at data points A and B illustrate the impact of "Parameter a" under the Reference condition of "Parameter b" (black dots). As "Parameter a" increased, the deblurred

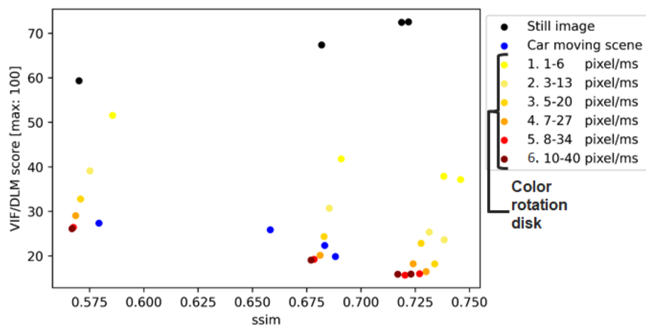

Figure 5: The result of VIF-DLM combined score vs SSIM. Only still images show a positive correlation. Simulation conditions were the same as the black plot in Fig. 4. .

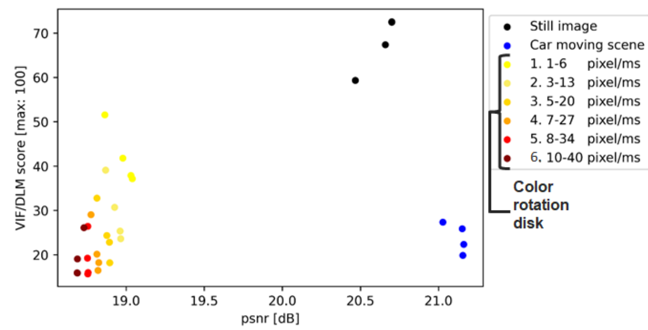

Figure 6: The result of VIF-DLM combined scores vs PSNR. Only still images also show a positive correlation. Simulation conditions were the same as the black plot in Fig. 4.

image became less noisy due to a reduction in noise events. However, the increase in "Parameter a" also resulted in greater blurriness in the deblurred image. This blurriness was attributed to the increased latency of event firing, which negatively affected the image quality and caused a lower VIF-DLM combined score. In addition to that, the deblurred image at data point C shows the impact of "Parameter b" in comparison to data point A. When "Parameter b" was raised to ten times the Reference condition, the deblurred image became more noisy than the one at data point A. This increase in noisiness was attributed to the heightened noise events caused by expanding the bandwidth of the EVS pixel circuit. As a result, this greater noise level led to a lower VIF-DLM combined score.

In summary, a low VIF-DLM combined score occured when the image was either noisy (as seen in C in Fig. 4) or blurry (B in Fig. 4). Conversely, a higher VIF-DLM combined score indicated both less noise and less blurriness, as viewed through an eye observation. The observations from Fig. 4 demonstrate that the VIF-DLM combined score for moving scenes can effectively evaluate blurriness and noise simultaneously.

Image quality metrics benchmarking

We further evaluated the VIF and DLM metrics for deblurred images alongside the Structural Similarity Index (SSIM) and the Peak Signal-to-Noise Ratio (PSNR), incorporating varying EVS pixel parameters. Figure. 5 illustrates the correlation between the combined scores of VIF and DLM with SSIM for assessing blurriness evaluation. Additionally, Fig. 6 shows the correlation between the combined scores of VIF and DLM with PSNR for evaluating noise. The deblurred images represented in these plots were obtained by varying the parameters of the EVS circuit, specifically "Parameter a" and "Parameter b" which were the same settings parameters utilized to create the black plot in Fig. 4. For this study, "Parameter b" was set to the "Ref" condition, while only "Parameter a" was varied. The deblurred images depicted in Fig. 5 and Fig. 6 are shown in Fig. 7 including a "No motion scene (Still image)", a "Natural motion scene (Car moving scene)," and "Controlled motion scenes (Color rotation disk)".

The black plots in Fig. 5 and Fig. 6 illustrate the correlation between the combined scores of VIF and DLM with the SSIM for "Still image". Since there was no motion present, the deblurred images did not exhibit any blurriness. We found that the combined VIF-DLM scores are positively correlated with both of SSIM and

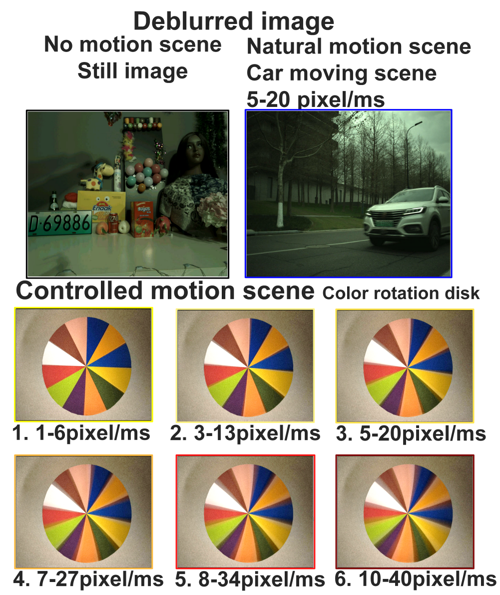

Figure 7: The deblurred images for a correlation study between the metrics. The images were generated at 20 Lux on the scenes. The condition of event generation used for this deblurring images is the condition of data point B in Fig. 4

PSNR due to the influence of noise on images. The noise characteristics were similar to those observed in the images from the "Car moving scene" as shown in Fig. 4. This indicates that as "Parameter a" increased, the resulting image displayed less noise. As a result, for the "Still image", the higher the produced combined VIF-DLM scores, the higher the SSIM and PSNR scores.

In contrast, the deblurred images from the "Car moving scene" exhibited noticeable blurriness, particularly of the vehicle due to an object motion, as depicted in Fig. 7. The blue plots in Fig. 5 and Fig. 6 show the results of the deblurred images for the "Car moving scene". These images were the ones studied VIF and DLM to assess blurriness and noise which were illustrated as the black plot in Fig. 4, indicating that as "Parameter a" increases, the images appear blurrier and less noisy upon visual inspection, resulting in lower VIF-DLM combined scores. Consequently, the VIF-DLM combined scores are negatively correlated with SSIM, as shown in Fig. 5. This indicates that SSIM fails to accurately recognize blurriness in noisy images. In Fig. 6, the PSNR values for the "Car moving scene" show a weaker correlation with the VIF-DLM combined score. Despite the changes in VIF-DLM combined scores, the PSNR values remained relatively consistent across all blue plots. This consistency can be explained by referring to the results from the "Car moving scene" which were represented by the black plots in Fig. 4. The figure illustrated that the lower VIF-DLM combined scores of the "Car moving scene" were due to blurriness in the images, despite them being relatively less noisy. As a result, the increase in blurriness counteracted the improvement in PSNR associated with noise reduction, leading to only a minor overall change in PSNR.

In addition to the "Car moving scene" analysis as a motion scene, we also examined blurriness in the other deblurred images using a "Color rotation disk" as a controlled motion scene by varying its rotation speed. Higher rotation speeds resulted in increased blurriness of the deblurred images. Figure 5 and Fig. 6 illustrate the correlation between the combined VIF and DLM scores with SSIM and PSNR, incorporating varying blurriness in the images of "Color rotation disk". We generated six different rotation speeds, represented by red-tinted plots (ranging from yellow to dark red), which were defined from the point where 20 percent to 80 percent of the disk's radius. The noise and blurriness in the deblurred images of the "Color rotation disk" exhibited a similar trend to that observed in the "Car moving scene". Consequently, the correlation between the combined scores of VIF and DLM with SSIM and PSNR for each rotation speed of the "Color rotation disk" displayed behavior similar to that of the "Car moving scene". Another observation from both Fig. 5 and Fig. 6 was that the VIF-DLM combined scores were positively correlated with SSIM and PSNR for the images from the "Color rotation disk" depicted in adjacent color plots, where the rotation speed was varied while maintaining consistent noise levels. These correlation results suggested that lower SSIM and PSNR scores were associated with greater blurriness when noise levels remain constant. This evaluation revealed that SSIM and PSNR could not assess noise and blurriness simultaneously; they need to be evaluated separately.

Based on the results from Fig. 4, Fig. 5, and Fig. 6, we concluded that VIF and DLM were suitable for End-to-End IQ simulation, as these metrics could simultaneously evaluate both blurriness and noise in motion scenes.

Pixel-speed assesment

Evaluation method

We quantified the distribution of pixel motion, which directly affected the blurriness in deblurred motion images. Our hypothesis was that the blurriness distribution in images correlated with the combined VIF-DLM score. The correlation between the VIF-DLM combined score for a natural motion scene and the score for a color rotation disk could represent the distribution of pixel motion. We prepared the scenes containing different areas of motion, as shown in Fig. 8. A "Color rotation disk" was utilized to identify the corresponding pixel speed distribution by varying the rotation speed. We found that the motion area of the "Car moving scene" was relatively closer to that of a color rotation disk. To assess pixel speed, we first compared the VIF-DLM combined score of deblurred images from "Car moving scene" with that of "Color rotation disk" images generated at different rotation speeds. Next, we applied the BEW to evaluate the blurriness of all color boundary edges from the center to the edge of the "Color rotation disk" for each rotation speed and derived the correlation between the combined VIF-DLM score and the BEW.

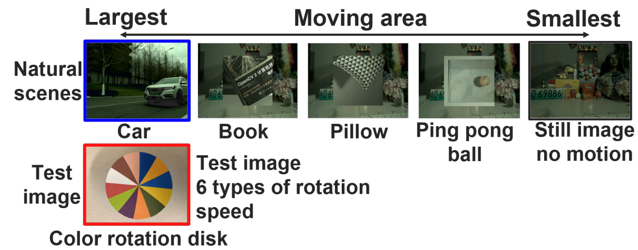

Figure 8: Data set used for this study. Images used for VIF/DLM and BEW by changing the ratio of the amount of still image area in the scene. Color-rotation-disk test moving scenes were used to evaluate natural motion scenes.

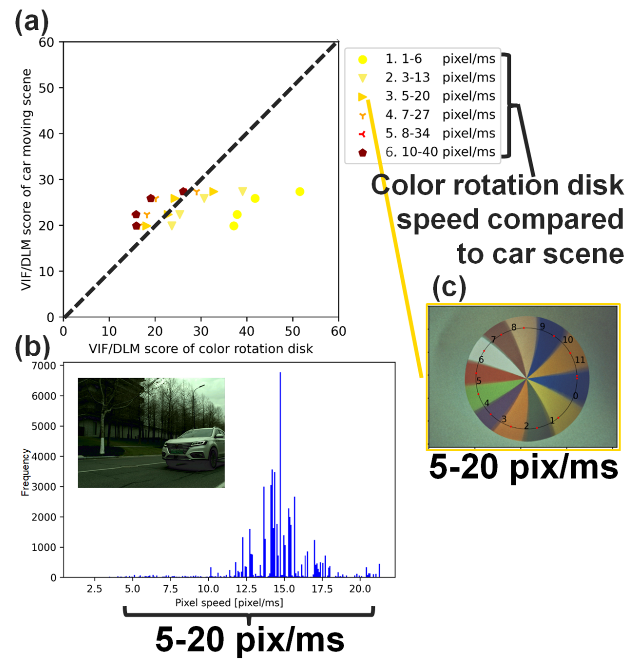

Figure 9: (a) VIF/DLM comparison between a car moving scene and color-rotation-disk images with different rotation speeds at 20 Lux on the scenes. The data is the same one in Fig.6. (b) Pixel speed distribution of a car moving scene in pixel/ms. The range is 5-20 pixel/ms. (c) Image of a color-rotation-disk image at pixel speed of 5-20 pixel/ms.

Pixel-speed assessment for natural motion scene

We determined the rotation speed of the color rotation disk by matching the VIF-DLM combined score between the "Car moving scene" image and each rotation speed of the "Color rotation disk" image. Figure. 9 (a) compares the VIF-DLM combined scores for the "Car moving scene" image against each rotation speed of the "Color rotation disk" image. Each "Color rotation disk" image was evaluated at a specified rotation speed in comparison to the "Car moving scene" image. All data sets presented in this graph were the same as those shown in Fig. 5. The pixel speed distribution of the "Color rotation disk" closely matched that of the "Car moving scene", specifically in the range of 5-20

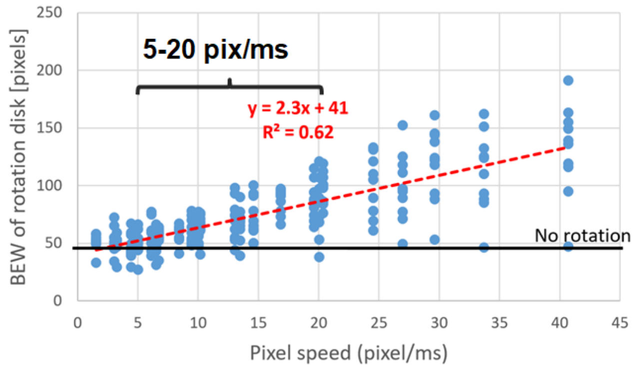

Figure 10: Correlation between BEW of rotation disk and its pixel speed.

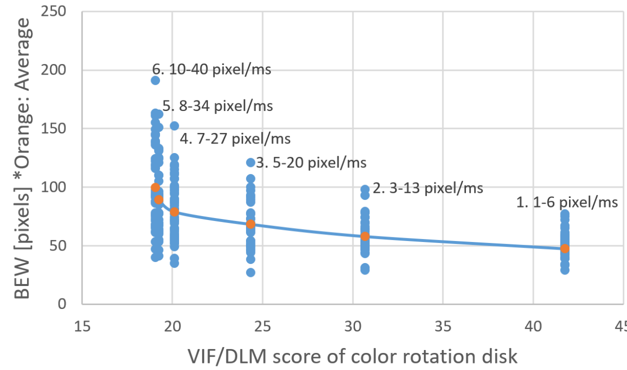

Figure 11: Correlation between BEW of rotation disk and its VIF-DLM combined score.

pixel/ms derived from a pixel-speed distribution shown in Fig. 9 (b). Under these conditions, the VIF-DLM combined score for the "Car moving scene" was similar to that for the "Color rotation disk" (refer to No.3 in Fig. 9 (a), and Fig. 9 (c)). On average, this VIF-DLM combined score was 25 points. We also analyzed the pixel speed of the "Color rotation disk" to quantify its blurriness. Figure 10 shows the correlation between the pixel speed of a rotating disk and its BEW. BEWs were extracted from six different rotation speeds of the "Color Rotation Disk" at all color boundary edges, specifically from 20 percent to 80 percent of the disk's radius. The averaged BEW at each rotation speed was found to be proportional to the pixel speeds. Furthermore, we also derived the correlation between the combined VIF-DLM score and the BEW obtained from the "Color rotation disk" as shown in Fig. 11. As discussed in Fig. 9, the average VIF-DLM score was 25 for the pixel speed distribution that is similar between the "Color rotation disk" and the "Car moving scene". This socre correlated with a BEW range from 50 to 120 in Fig. 11. This BEW range corresponded to a pixel speed of 5 to 20 pixel/ms, as indicated in Fig. 10, which is also the pixel speed range of the "Car moving scene" as shown in Fig. 9 (c). Therefore, from Fig. 10 and Fig. 11, we could estimate the pixel speed range of the "Car moving scene".

In summary, to evaluate the distribution of pixel speed for natural motion scenes based on these results, we can follow these steps:

1. Under a specific synthesized condition for both the deblurred color rotation disk image and the natural motion scene, determine the rotation speed of the color rotation disk that produces the combined VIF/DLM score similar to that of the natural motion scene. This will allow us to quantify the pixel speed distribution in natural motion scenes.
2. Once we have identified the rotation speed of the color rotation disk, we can assess the level of blurriness by measuring the BEW of the color rotation disk. Alternatively, we can use the determined combined VIF/DLM score of the color rotation disk, as explained in section "1." above, to estimate the blurriness. The BEW of the color rotation disk can be correlated with the VIF-DLM combined score by creating a graph that illustrates the relationship between the combined VIF-DLM score and the BEW. Analyzing the color rotation disk will provide us with an estimated pixel speed distribution for natural motion scenes.

This scheme can be performed to cross-check a blurriness evaluated from VIF/DLM.

Conclusion

We proposed an evaluation scheme by using both the VIF-DLM combined metric and BEW. We confirmed that the combined score of VIF-DLM detected both blurriness and noise in natural motion scene images at the same time. We also introduced a method to evaluate the distribution of scene pixel speed, which affects blurriness, by utilizing the correlation between BEW and VIF-DLM combined score. Through this IQ simulation with VIF-DLM combined metric and BEW, we realized an End-to-End IQ simulation scheme for natural motion scenes. This will enable circuit designers to specify EVS hardware parameters by simulating the influence on the finished images with a quantitative IQ metric before starting the hardware design.

References

[1] G. Gallego, T. Delbruck, G. Orchard, C. Bartolozzi, B. Taba, A. Censi, S. Leutenegger, A. Davidson, Joerg Conradt, K. Daniilidis, and D. Scaramuzza, "Event-based vision: A survey," in IEEE Transactions on Pattern Analysis and Machine Intelligence, 2020.

[2] P. Lichtensteiner and T. Delbruck, "A 64x64 AER logarithmic temporal derivative silicon retina," Research in Microelectronics and Electronics, 2005 PhD, 2005, pp. 202-205

[3] L. Pan, C. Scheerlinck, X. Yu, R. Hartley, M. Liu and Y. Dai, "Bringing a Blurry Frame Alive at High Frame-Rate With an Event Camera," 2019 IEEE/CVF Conference on Computer Vision and Pattern Recognition (CVPR), Long Beach, CA, USA, 2019, pp. 6813-6822, doi: 10.1109/CVPR.2019.00698.

[4] Hai Dinh, Qinyi Wang, Fangwen Tu, Brett Frymire, Bo Mu, "Evaluation of motion blur image quality in video frame interpolation," in Electronic Imaging, 2023, pp 262–1 - 262-5, https://doi.org/10.2352/EI.2023.35.8.IQSP-262.

[5] H. R. Sheikh and A. C. Bovik, "Image information and visual quality," in IEEE Transactions on Image Processing, vol. 15, no. 2, pp. 430-444, Feb. 2006, doi: 10.1109/TIP.2005.859378.

[6] S. Li, F. Zhang, L. Ma and K. N. Ngan, "Image Quality Assessment by Separately Evaluating Detail Losses and Additive Impairments," in IEEE Transactions on Multimedia, vol. 13, no. 5, pp. 935-949, Oct. 2011, doi: 10.1109/TMM.2011.2152382.

[7] Xiaozheng Mou, Kaijun Feng, Alex Yi, Steve Wang, Huan Chen, Xiaoqin Hu, Menghan Guo, Shoushun Chen, Andreas Suess, "Accurate event simulation using high-speed video," in Proc. IST Int'l. Symp.

on Electronic Imaging: Imaging Sensors and Systems, 2022, pp 242-1 - 242-6, https://doi.org/10.2352/EI.2022.34.7.ISS-242.
[8] R. Rassool, "VMAF reproducibility: Validating a perceptual practical video quality metric," 2017 IEEE International Symposium on Broadband Multimedia Systems and Broadcasting (BMSB), Cagliari, Italy, 2017, pp. 1-2, doi: 10.1109/BMSB.2017.7986143.
[9] C.Cortes and V.Vapnik, "Support-Vector Networks," Machine Learning, vol. 20, no. 3, pp. 273–297, 1995.

Author Biography

Daisuke Saito received his M.E. degree in applied physics from Tsukuba University, Tsukuba, Japan. He is currently a Staff System-on-Chip Modeling Engineer in the CTO Office at OmniVision Technologies, Inc. focusing on event vision-based sensor systems simulations and edge AI sensors.